The pressure-induced ferroelastic phase transition of SiO_2 stishovite

1995 J. Phys.: Condens. Matter 7 3693

(http://iopscience.iop.org/0953-8984/7/19/003)

J. Phys.: Condens. Matter 7 (1995) 3693–3698. Printed in the UK

The pressure-induced ferroelastic phase transition of SiO_2 stishovite

Changyol Lee†§ and Xavier Gonze‡

† Laboratory of Atomic and Solid State Physics, Cornell University, Ithaca, NY 14853-2501, USA

‡ Unité de Physico-Chimie et de Physique des Matériaux, Université Catholique de Louvain, B-1348 Louvain-la-Neuve, Belgium

Received 19 December 1994

Abstract. Using a newly developed accurate *ab initio* technique, we study the stability and the lattice dynamics of SiO_2 polymorph stishovite as a function of pressure. We observe a *ferroelastic* phase transition to $CaCl_2$ structure at 64 GPa, driven by a mechanical instability associated with a vanishing shear modulus. Other lattice instabilities due to phonon anomalies are theoretically excluded along with a proposed softening of the B_{1g} phonon mode.

As silicon and oxygen are the most abundant atomic species inside the earth, understanding the physics of silica (SiO_2) is especially relevant for geophysics and geochemistry. Studies of stishovite, a high-pressure form of SiO_2 with rutile structure, and its comparison to $Mg_{1-x}Fe_xSiO_3$ and to SiO_2 and MgO mixtures, help understand the constitution of the lower mantle of the earth. However, the range of stability of stishovite is still controversial and the structure of the post-stishovite phase is not yet well established.

High-pressure experiments to observe the structural transformation of stishovite are rather difficult due to the small size of available stishovite monocrystals, typically smaller than 0.5 mm, and the resulting set of the experimental data shows a large dispersion. Early experiments reported α-PbO_2 [1] or hexagonal Fe_2N structure [2], although the stability of those structures has yet to be confirmed. More recently, from the Raman spectra of stishovite up to 32.8 GPa, Hemley [3] deduced a transition to $CaCl_2$ structure at about 100 GPa via softening of the B_{1g} vibration mode. A reversible (unquenchable) distortion of stishovite was observed between 79 and 98 GPa, which was interpreted as a phase transition to $CaCl_2$ structure with a possibility of another type of distortion. On the other hand, there have been various theoretical predictions for the pressure-induced phase transition of stishovite using an electron gas model [5], a shell model [6], molecular dynamics simulations [7], or first-principles total energy calculations [8, 9]. Molecular dynamics simulations using semi-empirical pair potentials suggested that stishovite should be stable up to 250 GPa before transforming into the $CaCl_2$ structure [7]. Density functional calculations find that the $Pa\bar{3}$ structure [8] or $CaCl_2$ structure [9] has lower energy than stishovite above 60 GPa and 45 GPa, respectively, suggesting that the eightfold fluorite structure [10], higher in energy, could not be an immediate post-stishovite phase. However, accurate transition pressure and mechanism are difficult to predict from subtle energy differences alone.

§ Present address: Department of Physics, Ewha Women's University, Seoul 120-750, South Korea.

0953-8984/95/193693+06$19.50

In this work, we directly and accurately characterize the stability of stishovite using the variational density functional perturbation theory (VDFPT) [11–16]. We analyse the pressure-dependent phonon *band* structure and show that stishovite in the rutile structure is unstable with respect to a tetragonal to orthorhombic distortion before the frequency of the B_{1g} mode becomes imaginary, which suggests that an increase of hydrostatic pressure drives stishovite to $CaCl_2$ structure. We also analyse the nature of the associated second-order phase transition at 64 GPa, where the corresponding shear modulus vanishes. Such a spontaneous symmetry-breaking strain phenomenon is referred to as *ferroelasticity* [17] and shares similarity with ferromagnetism or ferroelectricity. The macroscopic strain due to the ferroelastic instability strongly couples with the microscopic atomic displacements in the B_{1g} mode, which is no longer soft in the $CaCl_2$ structure. The phonon band structure calculation allows us to exclude any other lattice instabilities due to phonon anomalies under hydrostatic compression.

VDFPT combines state of the art *ab initio* total energy algorithms [18, 19] and powerful variational principles within density functional perturbation theory [16]. VDFPT allows direct access to the second-order derivatives of the total energy with respect to atomic displacements and electric fields and does not require supercell computations. We obtain from VDFPT the Born effective charges, the electronic dielectric constant tensors, the phonon band structure, and the interatomic force constants to study the lattice dynamics and the structural stability of materials with both covalent and long-range dipole–dipole interactions. VDFPT has been applied to various oxides and perovskite materials [11–15] where theoretically calculated vibrational frequencies are shown to agree with experimental data at the level of a few per cent without any adjustable parameters. Further technical details including the choice of the basis set and the atomic pseudopotentials can be found in [15].

We begin with a computation of the structural parameters of stishovite as a function of pressure from the *ab initio* total energy calculations [18, 19]. Stishovite has a tetragonal unit cell with Si atoms at (0, 0, 0) and $(\frac{1}{2}, \frac{1}{2}, \frac{1}{2})$ and O atoms at $(u, u, 0)$, $(1-u, 1-u, 0)$, $(\frac{1}{2}-u, \frac{1}{2}+u, \frac{1}{2})$, and $(\frac{1}{2}+u, \frac{1}{2}-u, \frac{1}{2})$. For a given volume, we optimize the structural degrees of freedom a, c, and u of the unit cell and calculate the total energy. Then, we fit the optimized total energies by the Murnaghan equation of state [20]. We obtain from the fitted equation of state the equilibrium volume V_0, the lattice constants a and c, the internal parameter u, the bulk modulus B_0, and the pressure derivative of bulk modulus B_0' at zero pressure as shown in table 1. The calculated structural parameters and the equation of state compare favourably with experiment, and will be used for further investigation. It should be noted that experimental values of B_0' have a wide range [21]. For pressures equal to 0, 18, 42, 73, and 114 GPa, respectively, the value of u is 0.3052, 0.3036, 0.3024, 0.3014, and 0.3005, and the ratio c/a is 0.6421, 0.6471, 0.6503, 0.6524, and 0.6537. Therefore, Si–O bond lengths decrease with increasing pressure and stishovite is more compressible along the a direction than along the c direction, like other rutile-structured compounds.

Next, using the VDFPT, we calculate the phonon frequencies of stishovite at the Γ point at 0, 18, 42, 73, 114 GPa and the phonon *band* structure at 0 and 73 GPa, assuming the rutile structure. In table 2, we show the frequencies at the Γ point and calculate their pressure shifts. Hemley [3] observed the linear shifts in B_{1g}, E_g, and A_{1g} modes up to 32.8 GPa with the measured values -1.20, 1.93, and 3.39 cm^{-1} GPa^{-1}, respectively. These experimental data agree well with the calculated values. It is notable that the order of the phonon frequencies changes as the pressure increases. The frequency of the B_{1g} mode decreases with increasing pressure and vanishes at 86 GPa, while all other frequencies increase. We find a linear dependence of the square of the B_{1g} phonon mode frequency as

Table 1. Structural parameters of stishovite. Experimental data are from [29] except u which is from [30].

Property	This work	Experiment
a (Å)	4.14	4.1801
c (Å)	2.66	2.6678
u	0.3052	0.3062
V_0 (Å^3)	45.54	46.615
B_0 (GPa)	319.6	313.0
B_0'	3.87	1.7

Table 2. Pressure dependence of phonon frequencies ν of stishovite. Rutile structure is assumed unless otherwise stated. Frequencies are in cm^{-1} and i is $\sqrt{-1}$. Pressure shifts dν/dP are calculated in cm^{-1} GPa^{-1} from the data up to 18 GPa.

Mode	0 GPa	0 GPa[a]	18 GPa	42 GPa	73 GPa	73 GPa[b]	114 GPa	dν/dP
Raman modes								
B_{1g}	214.0	234	190.6	156.1	85.2	219.7	124.6i	−1.28
E_g	585.4	586	622.8	664.8	711.6	690.5, 702.3	763.3	2.04
A_{1g}	754.9	751	809.8	873.9	946.5	928.5	1028.7	3.00
B_{2g}	954.1	964	1021.9	1096.5	1178.4	1163.1	1267.6	3.70
Infrared modes								
E_u (TO)	469.0	470	492.4	510.7	526.6	518.6, 537.9	540.7	1.28
E_u (LO)	568.9	565	607.2	642.0	672.7	648.0, 696 6	700.1	2.09
E_u (TO)	595.1	580	673.7	743.9	804.8	801 1, 805.4	861.3	4.30
E_u (LO)	705.0	700	738.9	777.0	819.3	807.1, 826.8	866.6	1.85
A_{2u} (TO)	648.8	650	689.7	739.7	797.6	778.9	864.0	2.23
A_{2u} (LO)	1048.5	950	1090.9	1140.4	1196.5	1181.2	1259.9	2.32
E_u (TO)	821.6	820	868.7	935.4	1020.3	996.8, 1022.9	1121.2	2.57
E_u (LO)	1043.4	1020	1109.4	1185.0	1269.6	1259.7, 1264.9	1364.3	3.61
Silent modes								
B_{1u}	383.6	silent	399.0	414.3	429.6	424.1	443.5	0.84
A_{2g}	599.1	silent	631.0	665.0	700.7	713.2	736.7	1.74
B_{1u}	761.4	silent	815.4	877.1	946.7	926.8	1024.3	2.95

[a]Experimental data from [27] for Raman and [28] for infrared modes.
[b]In $CaCl_2$ structure. Mode assignments are made by comparison of the eigenvectors.

a function of pressure, as shown in figure 1. The eigenmodes can be classified into modes with atomic displacements only along the c direction (E_g, B_{1u}, and A_{2u}) and modes with atomic displacements only perpendicular to the c direction (all others). There is no apparent correlation between the magnitudes of pressure shifts and the above-defined categories of the eigenmodes contrary to the assertion in [3]. The atomic displacements in the B_{1g} mode consist of rigid rotations of O octahedra around Si atoms within the a–b plane.

The phonon *band* structures were calculated following a generalization of the technique used in [22]: first, we compute the dynamical matrices on the $(2, 2, 4)$ grid of phonon wavevectors in the reciprocal space [23] and apply Fourier transformation in order to get the interatomic forces. The long-range dipole–dipole interactions are taken into account separately the using calculated anisotropic Born effective charge tensor and dielectric tensor. The interatomic force constants are then used for generating the phonon spectra at *any* point in the Brillouin zone. In figure 2, we show the phonon spectra of stishovite with rutile structure at both 0 and 73 GPa along high-symmetry lines in the Brillouin zone. At 73 GPa,

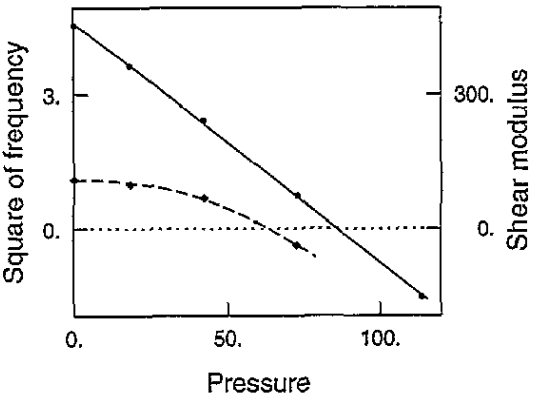

Figure 1. Pressure dependence of the shear modulus (diamonds) and the square of the B_{1g} phonon frequency (dots). Units are $10^4 \times cm^{-2}$ for the square of the phonon frequency, and GPa for the shear modulus and the pressure. Curves are guides to the eyes.

we can see that the B_{1g} mode at the Γ point approaches zero frequency and that all the modes have positive frequencies *except* an acoustic mode along the Γ–M line. (The imaginary frequencies are represented as negative in figure 2.) This important unstable acoustic mode is transverse in the *a–b* plane, thus directly associated with the tetragonal to orthorhombic shear distortion [24]. We therefore find that, although the frequency of the B_{1g} mode in the rutile structure vanishes at 86 GPa, the rutile structure is already unstable with respect to the orthorhombic distortion below 73 GPa. This is in agreement with the general observation by Miller and Axe [25] that an elastic instability must occur before a Raman-active optical mode softens completely. We do not find any other lattice instabilities with respect to mechanical perturbations of arbitrary wavelengths and symmetries under hydrostatic pressure, which would appear as imaginary frequencies in the phonon bands.

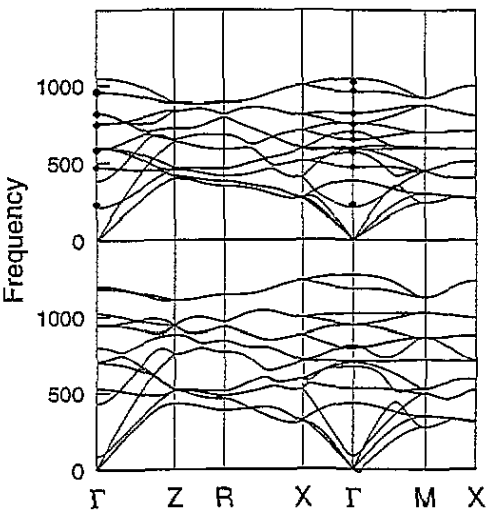

Figure 2. The phonon dispersion over the whole Brillouin zone at 0 (top) and 73 GPa (bottom). Frequencies are in cm^{-1}. Diamonds represent experimental data from [27] and [28].

In order to determine the pressure of the transition accurately, we now focus on the

analysis of the shear modulus due to the tetragonal to orthorhombic distortion as a function of pressure. Although the direct calculation of shear moduli could be performed within VDFPT, we use the more economical frozen-strain method [9]. Total energy calculations show that the tetragonal rutile structure is energetically preferred at 0, 18, and 42 GPa, with the positive shear moduli. The shear modulus becomes negative at 64 GPa, as shown in figure 1, indicating spontaneous distortion and a phase transition to $CaCl_2$ structure at 64 GPa. When relaxed at 73 GPa, the tetragonal unit cell with $a = b = 3.90$ Å and $u = 0.3014$ transforms into the lower-symmetry orthorhombic unit cell with $a = 3.83$ Å, $b = 3.97$ Å, and O atoms at $(u_1, u_2, 0)$, $(1 - u_1, 1 - u_2, 0)$, $(\frac{1}{2} - u_1, \frac{1}{2} + u_2, \frac{1}{2})$, and $(\frac{1}{2} + u_1, \frac{1}{2} - u_2, \frac{1}{2})$, with internal parameters $u_1 = 0.2803$ and $u_2 = 0.3198$. We see that O atoms show finite displacements of the B_{1g} type, i.e., rigid rotations of O octahedra around Si atoms in the a–b plane, as soon as the spontaneous shear distortion emerges. The former B_{1g} mode, with the relaxed $CaCl_2$ structure at 73 GPa, is no longer soft, with frequency 219.7 cm^{-1}, as shown in table 2. At 114 GPa, the relaxation drives the tetragonal unit cell with $a = b = 3.82$ Å and $u = 0.3005$ to the orthorhombic unit cell with $a = 3.72$ Å, $b = 3.93$ Å, and internal parameters $u_1 = 0.2682$ and $u_2 = 0.3293$.

The order parameters in the ferroelastic phase transition are the macroscopic ferroelastic strain *and* the microscopic atomic displacement associated with the B_{1g} mode, which are coupled to each other via an internal strain coefficient [26]. We find the phase transition is second order because both the symmetry-breaking ferroelastic strain and the microscopic atomic displacements are zero below the transition pressure and continuously become finite above the transition pressure. This is in agreement with the experiment by Tsuchida and Yagi, which estimates the volume change with the transition is less than 1%. A similar structural transformation is known for $CaCl_2$ where $CaCl_2$ in the orthorhombic structure undergoes ferroelastic phase transition into the rutile structure at 491 K [26].

In conclusion, we have applied the *ab initio* VDFPT technique for the direct characterization of the stability of stishovite at high pressure. We have shown that stishovite is unstable with respect to a ferroelastic tetragonal to orthorhombic distortion above 64 GPa and transforms to $CaCl_2$ structure via a second-order phase transition before the B_{1g} mode softens completely. The phonon band structure calculation rules out other continuous structural phase transition associated with lattice instability. Finite microscopic atomic displacements of the B_{1g} type emerge above the transition pressure along with a spontaneous ferroelastic shear distortion and the frequency of the former B_{1g} mode is no longer small. Our result supports the experimental observation of Tsuchida and Yagi [4] and the theoretical calculation by Cohen [9].

Acknowledgments

This work is supported by the Cornell Theory Center and Corning Incorporated (CL) and FNRS–Belgium (XG). We thank Professor A L Ruoff for critical reading of the manuscript, D C Allan and Professor M P Teter at Corning Inc. for making the Corning code available for ground state calculation, and J-C Charlier for part of the coding of the interatomic force constant calculation. The computations were performed on an IBM RS-6000 at the Laboratory of Atomic and Solid State Physics, Cornell University.

References

[1] German V N, Podurets M A and Trunin R F 1973 *Sov. Phys.–JETP* **37** 107
[2] Liu L, Bassett W A and Sharry J 1978 *J. Geophys. Res.* **83** 2301

[3] Hemley R J 1987 *High-pressure Research in Mineral Physics* ed M H Manghnani and Y Syono (Tokyo: Terra) p 347
[4] Tsuchida Y and Yagi T 1989 *Nature* **340** 217
[5] Hemley R J, Jackson M J and Gordon R G 1985 *EOS Trans. AGU* **66** 358
[6] Striefler M E 1985 *EOS Trans. AGU* **66** 358
[7] Tsuneyuki S, Matsui Y, Aoki H and Tsukada M 1989 *Nature* **339** 209
[8] Park K T, Terakura K and Matsui Y 1988 *Nature* **336** 670
[9] Cohen R E 1992 *High-Pressure Research: Application to Earth and Planetary Sciences* ed Y Syono and M H Manghnani (Tokyo: Terra) p 425
[10] Al'tshuler L V, Podurets M A, Simakov G V and Trunin R F 1973 *Sov. Phys.–Solid State* **15** 969
Podurets M A, Simakov G V and Trunin R F 1990 *Izv. Acad. Sci. USSR, Phys. Solid Earth* **26** 295
[11] Gonze X, Allan D C and Teter M P 1992 *Phys. Rev. Lett.* **68** 3603
[12] Gonze X, Charlier J-C, Allan D C and Teter M P *Phys. Rev.* B **50** 13035
[13] Ghosez P, Gonze X and Michenaud J-P 1994 *Ferroelectrics* **153** 91
[14] Lee C and Gonze X 1994 *Phys. Rev.* B **49** 14730;
Lee C, Ghosez P and Gonze X 1994 *Phys. Rev.* B **50** 13379
[15] Lee C and Gonze X 1994 *Phys. Rev. Lett.* **72** 1686
[16] Gonze X unpublished
[17] Salje E K H 1990 *Phase Transition in Ferroelastic and Co-elastic Crystals* (Cambridge: Cambridge University Press)
[18] Kohn W and Sham L J 1965 *Phys. Rev.* **140** A1133
[19] Teter M P, Payne M C and Allan D C 1989 *Phys. Rev.* B **40** 12255
[20] Murnaghan F D 1944 *Proc. Natl Acad. Sci. USA* **30** 244
[21] See, for example, table III in
Keskar N R, Troullier N, Martins J L and Chelikowsky J R 1991 *Phys. Rev.* B **44** 4081
[22] Giannozzi P, de Gironcoli S, Pavone P and Baroni S 1991 *Phys. Rev.* B **43** 7231
[23] Monkhorst H J and Pack J D 1976 *Phys. Rev. B* **13** 5188
[24] Born M and Huang K 1954 *Dynamical Theory of Crystal Lattices* (Oxford: Clarendon) pp 229–40
[25] Miller P B and Axe J D 1967 *Phys. Rev.* **163** 924
[26] Unruh H-G, Mühlenberg D and Hahn Ch 1992 *Z. Phys.* B **86** 133
[27] Vigasina M F, Guseva E V and Orlov R Yu 1989 *Sov. Phys.–Solid State* **31** 747
[28] Hofmeister A M, Xu J and Akimoto S 1990 *Am. Mineral.* **75** 951
[29] Ross N L, Shu J, Hazen R M and Gasparik T 1990 *Am. Mineral.* **75** 739
[30] Sinclair W and Ringwood A E 1978 *Nature* **272** 714